# LANGMUIR

pubs.acs.org/Langmuir Article

# Microtubule Detachment in Gliding Motility Assays Limits the Performance of Kinesin-Driven Molecular Shuttles

Neda M. Bassir Kazeruni, Juan B. Rodriguez III, Gadiel Saper, and Henry Hess\*



Cite This: https://dx.doi.org/10.1021/acs.langmuir.0c01002



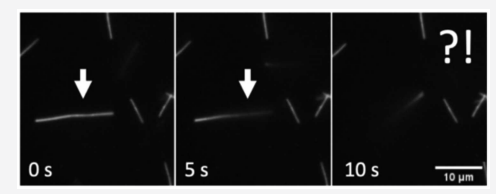
**ACCESS** 

Metrics & More

Article Recommendations

Supporting Information

**ABSTRACT:** The creation of complex active nanosystems integrating cytoskeletal filaments propelled by surface-adhered motor proteins often relies on the filaments' ability to glide over up to meter-long distances. While theoretical considerations support this ability, we show that microtubule detachment (either spontaneous or triggered by a microtubule crossing event) is a non-negligible phenomenon that has been overlooked until now. The average gliding distance before spontaneous detachment was measured to be  $30 \pm 10$  mm for a functional kinesin-1 density of



500  $\mu$ m<sup>-2</sup> and 9  $\pm$  4 mm for a functional kinesin-1 density of 100  $\mu$ m<sup>-2</sup> at 1 mM ATP. Even microtubules longer than 3  $\mu$ m detached, suggesting that spontaneous detachment is not caused by the stochastic absence of motors or their stochastic release due to a limited run length.

#### **■ INTRODUCTION**

A molecular shuttle<sup>1-5</sup> is a system capable of transporting molecules, vesicles, and other cargo from one location to another. Applications of such nanotransporters include biosensing, the study of collective motion, and biocomputation.8 One of the most widely studied molecular shuttles consists of cargo-carrying microtubules being propelled on a surface by physisorbed kinesin-1 motor proteins. 9,10 Devices integrating such molecular shuttles rely on microtubules remaining attached to the kinesin-covered surface as they are going from point to point. For instance, the biocomputation device described by Nicolau et al.8 requires microtubules to glide over two hundred micrometers with a negligible probability of detaching, because the arrival of the gliding microtubules at specific exits of a network of open channels indicates a specific output. Plans for future generations of this device rely upon uninterrupted microtubule gliding over distances up to one meter.

A theoretical analysis by Klumpp and Lipowsky<sup>11</sup> of the transport of nanoscale cargo by multiple kinesins along an immobilized microtubule can be applied to this inverse geometry (microtubules transported by immobilized kinesins). Similar to an earlier analysis by Hancock and Howard, 12 it predicts that the average distance a microtubule glides before detaching increases exponentially with the number of kinesin motors interacting with it, because individual motors have limited run lengths of the order of 1  $\mu$ m. <sup>13,14</sup> The model predictions are supported by experimental evidence for the transport of vesicles by 5-10 kinesin-1 motors on microtubules over millimeter distances. 11 However, for microtubules gliding on kinesin-coated surfaces, a much larger number of motors (10-1000) can simultaneously interact with a microtubule. For typical microtubule lengths  $^{7,15,16}$  of 5  $\mu$ m, a kinesin-microtubule interaction width 17 of 88 nm, and kinesin

densities  $^{18-21}$  between 20 and 1000  $\mu m^{-2}$ , the Klumpp and Lipowsky model predicts gliding distances between 0.2 and  $10^{17}$  m (10 light-years). For this reason, microtubule detachment during gliding is not expected to occur.

To our surprise, close examination of microtubule gliding on surfaces coated with a high density of kinesin-1 revealed a significant number of detachment events, where the microtubule leaves the surface. This prompted the present study, where we measure the rate of detachment events at different gliding velocities and motor densities. Contrary to the theoretical predictions, we find small but significant numbers of detachment events whose frequency increases with increasing velocity, decreasing motor surface density, and increasing duration of the experiment. This implies that the detachment of gliding filaments has to be considered in the design of nanodevices relying on the transport of cytoskeletal filaments by surface-adhered motor proteins.

# **■ THEORETICAL PREDICTIONS**

Spontaneous detachment at a high rate has been previously observed by Howard et al.<sup>19</sup> in experiments using very low densities of kinesin-1 and short microtubules, where it is highly likely that the microtubule will be unable to reach another kinesin before it unbinds from the last kinesin holding it. Because the kinesins are randomly distributed on the surface, the number of motors covered by a microtubule is Poisson-

Received: April 8, 2020 Revised: June 16, 2020 Published: June 17, 2020



distributed. Therefore, the probability P for a microtubule not to find another kinesin motor in its path before it unbinds is given by

$$P = e^{(-w\sigma L)} \tag{1}$$

where L is the length of the microtubule, w = 88 nm is the kinesin–microtubule interaction width, <sup>17</sup> and  $\sigma$  is the density of kinesins on the surface. The probability p for a microtubule not to detach from the surface after gliding a distance d is the cumulative probability of not detaching after each kinesin it encounters, which is given by

$$p(d) = (1 - P)^{w\sigma d} \tag{2}$$

The expected average gliding distance  $\langle d_{\rm H} \rangle$  is thus:

$$\langle d_{\rm H} \rangle = 1 / \left( w\sigma \times \ln \left( \frac{1}{1 - e^{-Lw\sigma}} \right) \right) \approx (e^{Lw\sigma} - 1) / w\sigma$$
 (3)

The theory by Klumpp and Lipowsky takes a complementary perspective by modeling a fixed number of kinesin motors transporting a particle along a microtubule and accounting for the limited and force-dependent run length of the individual kinesin motors. Their model vields an estimate for the average travel distance of  $5^{(n-1)}/n$   $\mu$ m, where n is the number of motors. This means that 10 motors can translate a particle 0.2 m without detaching. Applied to our situation where a certain number of kinesins attached to a surface (rather than the particle) interact with one microtubule, the number of motors n is given by  $Lw\sigma$ , and the average transport distance is

$$\langle d_{\rm KL} \rangle = 5^{Lw\sigma-1}/Lw\sigma \times 1 \,\mu{\rm m}$$
 (4)

The predictions of both theories for short (1  $\mu$ m) and long (10  $\mu$ m) microtubules are shown in Figure 1. The average

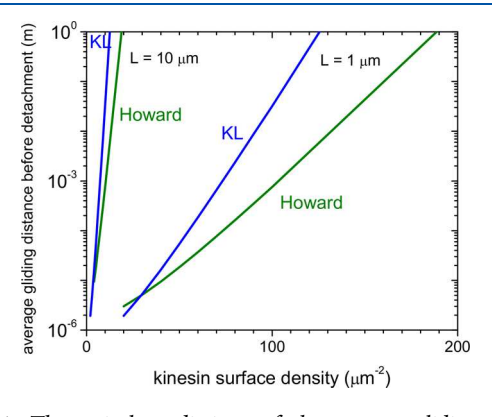


Figure 1. Theoretical predictions of the average gliding distance before microtubule detachment by the Howard model (eq 3) and the Klumpp–Lipowsky (KL) model (eq 4) assuming a kinesin–microtubule interaction width of 88 nm and microtubule lengths of 1 and 10  $\mu$ m.

gliding distance before detachment increases exponentially with motor density and microtubule length and reaches astronomically high values under the conditions used in the experiments described here and a value for the kinesin-microtubule interaction width of 88 nm.

Ideally, a complete theory aiming to describe the detachment of microtubules while gliding on kinesin-coated surfaces would simultaneously account for the random distribution of motors and their limited run length. The theory would likely

yield lower estimates than the two described approaches, but it would still predict an exponential dependence of the gliding distance on motor density and microtubule length. In terms of the detachment rate, a gliding distance which increases exponentially with motor density and microtubule length implies that primarily the shortest microtubules detach and only at the lowest motor densities. Neither the order of magnitude nor the functional dependence of the gliding distance matches the experimental measurements described in the following section.

# ■ EXPERIMENTAL RESULTS AND DISCUSSION

We observed the gliding of fluorescently labeled microtubules on full-length kinesin-1 physisorbed to casein-coated glass surfaces at kinesin densities of 100, 500, and 1000  $\mu m^{-2}$  (determined by landing rate measurements  $^{19,22}$  as described in the Supporting Information, section 1) and ATP concentrations of 0.01 and 1 mM (resulting in gliding velocities of 70–180 and 560–700 nm/s). By imaging the microtubules every 5 s, detachment events could be directly observed and manually counted.

Two types of detachment events can be observed in all experimental conditions: spontaneous detachment and crossinginduced detachment (Table 1). We define a detachment event as spontaneous when a microtubule leaves the surface without prior deformation due to an inactive kinesin or without another microtubule in its immediate vicinity (Figure 2a-d). The trajectories of spontaneously detaching microtubules were not significantly different from those of nondetaching microtubules and exhibited no obvious reasons for detachment, such as high curvature (Supporting Information, section 2). Crossing-induced detachment can occur when two microtubules collide and the bottom microtubule serves as a lever inducing the detachment of the second microtubule (Figure 2a). Previous studies of the crossing events have shown that 50–100% (depending on motor density) of the crossing microtubules pass over the other microtubule<sup>23-25</sup> but then rebind with the kinesin-coated surface on the other side. Here we find that the number of microtubules which fail to reconnect on the other side is small (the percentage of detaching microtubules varies from 0.33% to 10% for different experimental parameters) but not zero. We refer to these complete detachments as "crossing-induced detachments".

To understand what causes spontaneous detachment events, we first hypothesized that an obstacle on the surface induces the microtubules to leave the surface, replicating the mechanism for crossing-induced detachment (Figure 3a). We had to reject this hypothesis for four reasons: (1) We mapped the surface of our cleaned coverslips using a profilometer (Supporting Information, section 3). We calculated the roughness over a 10  $\mu$ m window corresponding to the length of the microtubules and determined an RMS value of 4 nm. Since a microtubule glides  $17 \pm 2$  nm above the surface for this type of kinesin, 26 it is highly unlikely that the microtubule will encounter a large enough obstacle to cause detachment. (2) While every square micrometer of the field of view is visited repeatedly (given an area of 6400  $\mu$ m<sup>2</sup> and about 1000 microtubules tracing out a path of about 80  $\mu$ m length), detachment events do not cluster. It thus appears that detachment is not triggered by crossing specific locations on the surface or that the sites would have to have nanoscale dimensions (so that they are found once but never twice). They would have to be significant obstacles to gliding, of which we found no evidence in our surface imaging. (3) The detachment events were randomly distributed on the surface. Using a method similar to the one used by Narayan et al.,<sup>27</sup> we found that the distribution of detachment events on the surface was uniform (Supporting Information, section 4). (4) Interference reflective microscopy (IRM) experiments<sup>28</sup> showed that (a) our cleaning method was adequate and no obstacle was introduced in the flow cell during its mounting and the flowing-in process and (b) we can observe both spontaneous and crossing-induced detachment events

Table 1. Observed Detachment Events, Crossing Events, Gliding Velocity, and Calculated Average Gliding Distance before Detachment for the Different Experimental Conditions in the Field-of-View (FOV) of 81  $\mu$ m  $\times$  81  $\mu$ m

						number of detachment events in 1800 s in FOV		
kinesin density $(\mu m^{-2})$	ATP concentration (mM)	average length of microtubules $(\mu m) \pm SD$	average gliding velocity (nm/s) ± SE	number of observed microtubules in FOV	number of crossing events in FOV	spontaneous	crossing- induced	average length of spontaneously detaching microtubules $(\mu m) \pm SD$
1000	1	$1.7 \pm 1.7$	$560 \pm 20$	1506	$460 \pm 40$	11	5	$1.0 \pm 0.7$
	0.01	$5.3 \pm 5.4$	$180 \pm 20$	1095	$300 \pm 30$	4	1	$1.5 \pm 1.2$
500	1	$3.9 \pm 3.3$	$670 \pm 20$	1178	$510 \pm 50$	39	29	$1.2 \pm 0.4$
	0.01	$5.9 \pm 6.0$	$70 \pm 6$	940	$310 \pm 40$	8	11	$2.8 \pm 1.6$
100	1	$2.6 \pm 2.4$	$700 \pm 60$	741	$150 \pm 20$	70	15	$2.4 \pm 1.0$
	0.01	$4.7 \pm 4.9$	$110 \pm 6$	1119	$260\pm30$	19	15	$7.7 \pm 1.4$

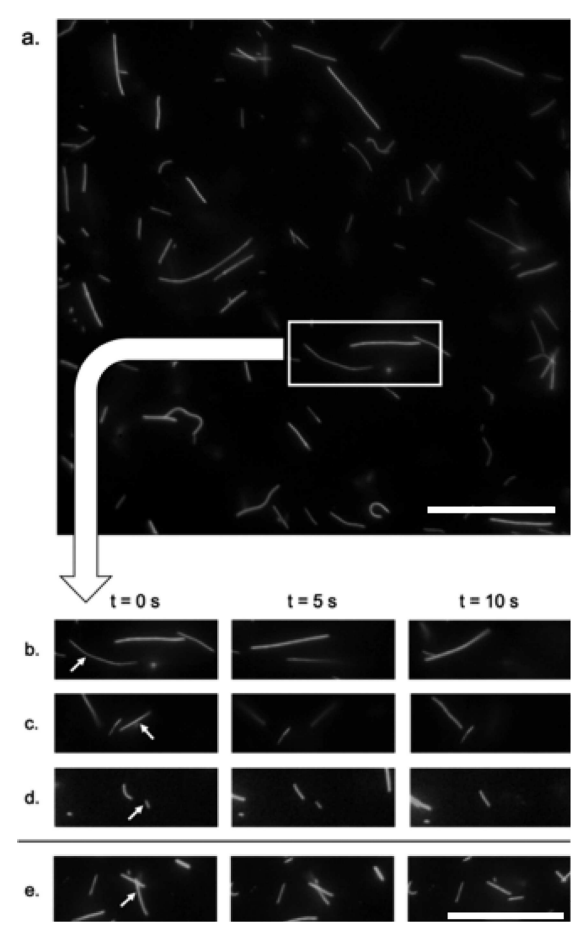


Figure 2. Fluorescence microscopy images of microtubule detachment. (a) An entire field of view. (b–d) Spontaneous microtubule detachment: long (10–20  $\mu$ m) (b), medium-length (5–10  $\mu$ m) (c), and short (0.5–2  $\mu$ m) (d) microtubules (marked with white arrows) gradually detach and leave the surface. All of the above microtubules are longer than 1  $\mu$ m. (e) Crossing-induced microtubule detachment. The vertical microtubule gradually detaches as it crosses over another. The kinesin density is 500  $\mu$ m<sup>-2</sup>, and the ATP concentration is 1 mM in all images. Scale bars: 20  $\mu$ m.

on sites on the flow cell that are obstacle-free (Supporting Information, section 5).

The temporal distribution of spontaneous detachment events was uniformly random (Figure 4a), but—since the number of gliding microtubules falls exponentially with time to a small fraction of the initial number over the course of the experiments—the rate of spontaneous microtubule detachment is not randomly distributed in time as a  $\chi$ -squared test (after removing outliers using the method of

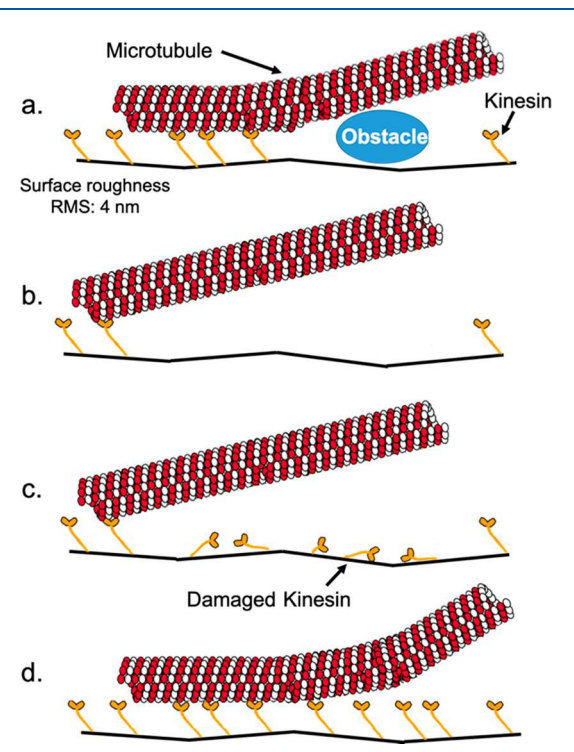


Figure 3. Potential causes of spontaneous microtubule detachment: (a) an obstacle on the surface leads to microtubule detachment; (b) a local depletion of kinesin motors provides microtubules with the opportunity to diffuse away from the surface and detach; (c) kinesin motors get damaged over time; (d) the microtubule changes conformation and leaves the surface of the flow cell.

Van Selst and Jolicoeur<sup>29</sup>) shows (Supporting Information, section 6). In fact, for the experimental conditions where we observe a high enough number of spontaneous detachments events to permit this analysis (100 and 500  $\mu$ m<sup>-2</sup> at 1 mM ATP), we find that the spontaneous detachment rate increases exponentially with time and that it increases roughly in inverse proportion to the motor density (Figure 4b).

The substantial decrease of the average gliding distance over time can result from photodamage due to the continuous fluorescence excitation,  $^{30,31}$  and by extrapolating the average gliding distance at each condition to time zero, we obtain an experimental average gliding distance to spontaneous detachment of 30  $\pm$  10 mm for 500  $\mu m^{-2}$  at 1 mM ATP and 9  $\pm$  4 mm for 100  $\mu m^{-2}$  at 1 mM ATP.

In IRM experiments where photodamage is absent,  $^{25,32,33}$  the number of gliding microtubules does not decline, but the number of counted detachment events is too small to conclude that they are not uniformly distributed. The average gliding distance measured in the IRM experiment for a motor density of 500  $\mu$ m<sup>-2</sup> and an ATP

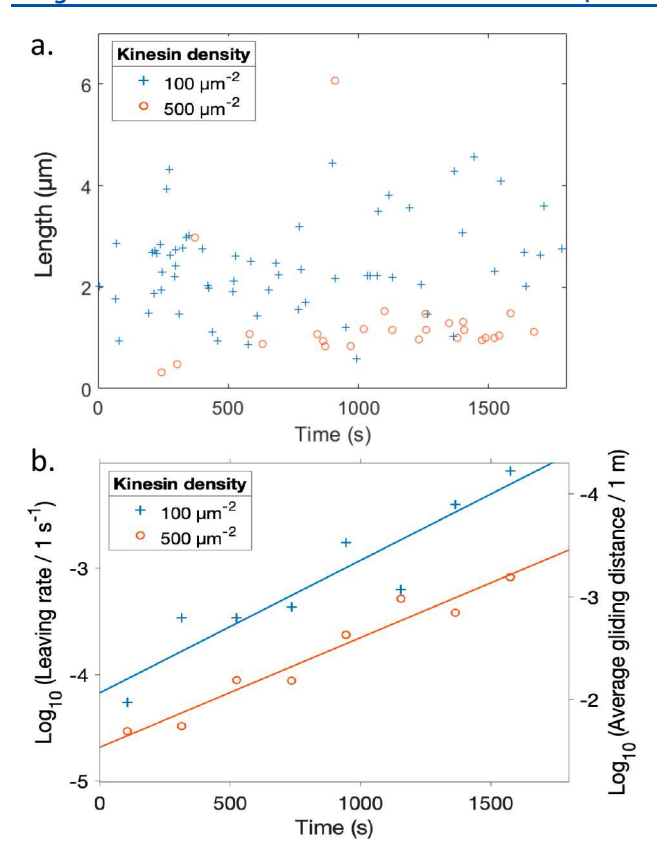


Figure 4. Spontaneous detachment at 1 mM ATP and kinesin densities of 100  $\mu$ m $^{-2}$  (blue crosses) and 500  $\mu$ m $^{-2}$  (red circles). (a) Lengths of detaching microtubules over time. Each symbol corresponds to an individual detachment event. (b) Spontaneous detachment rate over time for experiments with 1 mM ATP concentration. The logarithm of the detachment rate was fit using a linear regression.

concentration of 1 mM is  $28 \pm 14$  mm (error calculated by error propagation), which matches the extrapolated initial average gliding distance in the fluorescence microscopy experiment for this density and ATP concentration.

Interruptions in the smooth gliding of the microtubules<sup>34</sup> were observed by us, presumably due to interaction of the microtubule with defective kinesins (videos in the Supporting Information, described in Supporting Information section 8). However, these events were not correlated with the observed detachment events. Instead, these events are correlated to the breaking of microtubules, which is rare but not as rare as detachment. Since attachment events can also result from fluorophore-assisted light inactivation, exposure to excitation light can cause increased breaking and shortening of gliding microtubules. A linear decrease in the microtubule length over time in turn causes—according to either theory—exponentially increased detachment rates, which would explain the observations in Figure 4.

Unfortunately, we could not keep the microtubule length constant between the different experimental conditions. This difficulty arose because breaking and shrinking events rapidly alter the initial length distribution, for example shortening the microtubules for the 1 mM ATP experiments. Therefore, it is difficult to establish the exact dependence of the average gliding distance to spontaneous detachment on the microtubule length. However, it is clear from the widely varying average length of the detaching microtubules (Table 1) and the observed spontaneous detachment of longer microtubules (Figure 2b,c; Figure 4a) that the microtubule length does not have the dramatic effect ("primarily the shortest microtubules detach") predicted by either theory.

The reduction of the velocity arising from a reduced ATP concentration of 0.01 mM is correlated with a roughly proportional

decrease in the number of spontaneous detachment events (Table 1), which implies that the average gliding distance before spontaneous detachment is not strongly affected by the gliding velocity. This matches the predictions of both theories. The numbers of crossing-induced detachment events are small, which leads to large statistical errors when the small fractions of crossing events ending in detachment are calculated for the different experimental conditions, but there is no striking effect of either gliding velocity or motor density on the fraction of crossing events leading to detachment.

A reduction in the value of the kinesin-microtubule interaction width to about 20 nm places the theoretical gliding distance before detachment in the same range as the experimentally measured values. We chose a value for the kinesin-microtubule interaction width of 88 nm based on Palacci et al.<sup>17</sup> and a value for the microtubule width of 20 nm for the calibration of the kinesin surface density using landing rate measurements based on Dumont et al.<sup>21</sup> VanDelinder et al.'s recent measurements of the kinesin-microtubule interaction width at low motor densities (10-20  $\mu$ m<sup>-2</sup>) provide strong support for a kinesin-microtubule interaction width of 20 nm,<sup>35</sup> although their discussion also highlights the difficulties in determining motor densities and interaction widths at high motor densities. One could also argue that the kinesin-microtubule interaction width and the effective microtubule width used for motor density calculations from landing rate experiments should have the same value, because they are both related to a kinesin searching for a microtubule to bind to. The counter argument is that the gliding microtubule presents a nearly stationary target for the kinesin, whereas the freely diffusing microtubule is diffusing quickly and the kinesin is the target. While one should keep an open mind with respect to the correct value of the kinesin-microtubule interaction width, it is clear that no matter what the linear density of the motors along the microtubule is, the detachment rate should decrease exponentially with microtubule length. We do not find this exponential decrease (Figure 4a), thus neither one of the theories can provide a satisfying explanation.

The reviewers have commented on the relatively large number of microtubules which get temporarily or permanently stuck during gliding and interpreted this observation as an indication that the kinesin preparation is not perfect; that there is a substantial number of inactive motors on the surface. Furthermore, the reviewers pointed to the fluctuating ends of microtubules toward the end of some experiments (e.g., 0.01 mM and 100  $\mu$ m<sup>-2</sup>) as evidence of lower than stated motor densities. We are in complete agreement that the active motor density is dropping over the course of the experiments, with the shift between the 500 and the 100  $\mu$ m<sup>-2</sup> regression line in Figure 4b suggesting a roughly 5-fold reduction after 500 s. This implies a more than hundred-fold reduction from the initial motor density toward the end of the experiment, and the observation that the attachment points of a microtubule are separated by 10-20  $\mu$ m toward the end of the experiment is actually consistent with an initial density of 100  $\mu$ m<sup>-2</sup>. We account for the decreasing motor density by extrapolating toward time zero. However, just as the absence of an exponential dependence of detachment rates on microtubule length cannot be explained by the theories, the detachment rate appears not to be exponentially dependent on the motor density (which is itself falling exponentially over time in a first order process, such as desorption or inactivation by excitation light). In our opinion, the potential presence of inactive motors has the same practical effect as choosing a too large kinesin-microtubule interaction width: it shifts the values of the theoretical predictions but not their functional dependence on microtubule length and kinesin density, which are inconsistent with our experimental observations. A better kinesin preparation, e.g. by expressing the kinesin in insect cells rather than bacteria, is certainly helpful, 36 just not as much as predicted.

The origin of the spontaneous detachment may arise from the behavior of the microtubule rather than the binding of the kinesin modeled by Howard et al. and Klumpp and Lipowsky. Gosselin et al. suggested that microtubules have a preferred curvature, being either in a straight state; in a weakly curved state with radius of curvature of 10  $\mu$ m; or a highly curved state with radius of curvature of 1  $\mu$ m. <sup>37</sup> As a result of these states, microtubules sometimes move on the surface in

circular patterns rather than following a trajectory resembling a persistent random walk.<sup>38</sup> However, if a microtubule assumes one of its curved states so that it moves away from the surface of the flow cell, it would be gradually held by fewer and fewer kinesins and eventually fully detach from the surface (Figure 3d). The same mechanism may be responsible for crossing-induced detachment events, only instead of the initial detachment of the tip of the microtubule occurring randomly, it is caused by the "bottom" microtubule forcing the other one's tip to detach in order to be able to glide across it. The frequency of transitions between the straight states and the curved states of a microtubule are unknown, but curved states—which have to be distinguished from bending arising from a pinned microtubule tip—are rather rare in our experiments (videos in the Supporting Information, described in Supporting Information section 8). However, the observed weak dependence of the average gliding distance before spontaneous detachment on motor density, gliding velocity, and microtubule length is not obviously incommensurate with the idea that the spontaneous switching of the microtubule between straight and curved states leads to detachment events. An additional factor to consider is the potential role of lattice defects in the microtubules, which may interfere with continuous surface attachment.

The question how far a microtubule can glide before detaching has previously been experimentally studied on patterned surfaces, where surface sites or pillars carrying kinesin motors are separated by areas without kinesin.<sup>39,40</sup> Verma et al.<sup>41</sup> found that the gliding distance drops faster than expected when the spacing between the kinesin sites is increased, and conclude: "...thermal fluctuations of the filament tip normal to the surface decrease the probability that the microtubule will bind to motors immobilized on the surface. In addition, it can't be ruled out microtubules also have small degrees of curvature that cause the leading end to bend away from the surface. This microtubule curvature has been noted by others", <sup>42,43</sup> which introduces the idea of the microtubule bending away from the surface described in the previous paragraph.

The impact of spontaneous detachment after in average several centimeters of gliding on device performance depends on the design of the device. In a device such as the "smart dust biosensor", 6 where gliding microtubules capture, tag, and deposit an analyte, it limits the start-to-end distance covered in the process. In a device for analyte concentration, it limits the harvesting area. 44–47 In a biocomputation device, 8 it may cause an exponentially increasing loss of motile agents which compromises the accuracy of the output. The average gliding distance before detachment may be increased by utilizing higher motor densities, although higher motor densities have negative effects too, such as higher energy consumption and higher rates of microtubule shrinking. Our main point here though is that a limited gliding distance before spontaneous detachment has to be considered by the designer, whereas in the past the implicit assumption was that spontaneous detachment is not a factor.

# CONCLUSION

Microtubule detachment is a non-negligible phenomenon in gliding motility assays, limiting average gliding distances before detachment. The frequency of detachment events depends on both the kinesin density and the microtubules' gliding velocity, and microtubule detachment is more than 3 orders of magnitude more frequent than expected. Potential solutions to the problem of undesired detachment include partially covered channels, <sup>10,37</sup> and the use of microtubule bundles as motile agents, since it has been shown that addition of methylcellulose and the microtubule-associated protein MAP4<sup>48</sup> results in the formation of large-scale bundles that are less likely to detach. <sup>48,49</sup> In summary, detachment of gliding filaments has to be taken into account for the design of nanodevices incorporating cytoskeletal filaments propelled by surface-adhered biomolecular motors.

#### MATERIALS AND METHODS

**Microtubules.** These were polymerized from a 20  $\mu$ g aliquot of rhodamine-labeled, lyophilized tubulin (Cytoskeleton Inc., TL670M) with 6.25  $\mu$ L polymerization buffer. The polymerization buffer consisted of BRB80 buffer, with 4 mM magnesium chloride (MgCl<sub>2</sub>), 1 mM GTP, and 5% dimethyl sulfoxide. BRB80 buffer is composed of 80 mM piperazine-N,N'-bis(2-ethanesulfonic acid), 1 mM MgCl<sub>2</sub>, and 1 mM ethylene glycol tetraacetic acid (EGTA), adjusted to pH of 6.89 with potassium hydroxide (KOH). The resulting solution was then incubated on ice for 5 min before being transferred to a 37 °C water bath for 30 min. The microtubules were then diluted a hundred-fold into BRB80 buffer and stabilized with 10  $\mu$ M paclitaxel.

**Kinesin-1.** These from wild-type, full-length Drosophila was expressed by the team of G. Bachand at the Center for Integrated Nanotechnologies (Sandia National Laboratory) in *Escherichia coli* and purified using a Ni-NTA column. The kinesin was then nitrogen frozen in a buffer consisting of 40 mM imidazole, 300 mM NaCl, 0.76 g/L EGTA, 37.2 mg/L EDTA, 50 g/L sucrose, 0.2 mM TCEP, and 50  $\mu$ M Mg-ATP; the buffer being at pH 7. As measured from absorbance at 280 nm, the concentration of the kinesin is 3.16 mg/mL. The functional kinesin density was computed from landing rate experiments. The functional kinesin density was computed from landing rate of the concentration of kinesin would result in our flow cells in a surface density of 11 000  $\pm$  2000  $\mu$ m<sup>-2</sup>.

**Flow Cells.** These were assembled from a longer coverslip (60 mm  $\times$  25 mm) and a shorter one (22 mm  $\times$  22 mm), separated by two strips of double-sided adhesive tape. Before being assembled into flow cells, the coverslips were washed twice with ethanol, twice with ultrapure water, sonicated for 5 min, and dried in an oven at 75 °C.

Experimental Procedure. A solution of 0.5 mg/mL casein in BRB80 buffer was flowed into a flow cell. After 5 min, the solution was exchanged with the kinesin motor solution (kinesin to coat the surface with 100  $\pm$  20  $\mu m^{-2}$ , 500  $\pm$  100  $\mu m^{-2}$  or 1000  $\pm$  200  $\mu m^{-2}$ ; 0.5 mg/mL casein; 0.01 mM or 1 mM ATP), which in turn was exchanged after 5 min with the microtubule solution (16 nM tubulin, 0.5 mg/mL casein, 10 µM paclitaxel; 20 mM D-glucose, 20 µg/mL glucose oxidase, 8  $\mu$ g/mL catalase, 10 mM dithiothreitol and 0.01 or 1 mM ATP in BRB80). After another 5 min, the microtubule solution was exchanged with an enzymatic antifade solution (0.5 mg/mL casein, 10 µM paclitaxel; 20 mM D-glucose, 20 µg/mL glucose oxidase, 8 µg/mL catalase, 10 mM dithiothreitol and 0.01 or 1 mM ATP in BRB80)<sup>31,51</sup> in order to remove unbound microtubules from the solution. All experiments were performed at 24  $\pm$  1 °C. The initial length distribution of microtubules as well as its evolution throughout the experiment is provided in the Supporting Information, section 7.

Image Acquisition and Data Analysis. The flow cells were imaged using a Nikon TE2000-U epi-fluorescence microscope equipped with an iXON DU897 ultra electron-multiplying chargecoupled device (EMCCD) camera (Andor) and a 100× oil objective (NA = 1.45). For each flow cell, a field of view was randomly selected and images were taken every 2 or 5 s for 30 min. The exposure time was 200 ms for all images. Data analysis was conducted using FIESTA filament tracking software  $^{\rm 52}$  (available at https://www.bcube-dresden. de/fiesta/wiki/FIESTA) to measure the length and number of microtubules and ImageJ imaging software (available at http:// rsbweb.nih.gov/ij/) to visually identify single detachment events and determine the lengths of microtubules at that moment. The minimum length of tracked microtubules was set to 0.5  $\mu$ m. The number of crossing events was manually counted for one quadrant of the field of view for all images in an experiment and multiplied by four. Imaging started less than a minute after adding the antifade solution to the flow cell, and all 30 min of the video were analyzed. AVI videos of the conducted experiments are provided in the Supporting Information (described in Supporting Information section 8).

**IRM Experiment.** For the interference reflection microscopy measurements, a 50/50 mirror (Chroma) was used instead of the dichroic mirror as previously described by Mahamdeh et al. The sample was illuminated with a Sola light engine (Lumencore). The gilding assay was performed as described above.

# ASSOCIATED CONTENT

# **5** Supporting Information

The Supporting Information is available free of charge at https://pubs.acs.org/doi/10.1021/acs.langmuir.0c01002.

Determination of the surface density of kinesin using landing rate experiments. Profilometer analysis of a coverslip. Mapping the surface of the flow cell using IRM. Spatial distribution of detachment events. Temporal distribution of detachment events. Trajectories of detaching microtubules. Initial length distribution of microtubules and its evolution with time. (PDF) Experimental videos (AVIs)

# AUTHOR INFORMATION

# **Corresponding Author**

Henry Hess − Columbia University, New York, New York 10027, United States; orcid.org/0000-0002-5617-606X; Email: hh2374@columbia.edu

#### **Authors**

Neda M. Bassir Kazeruni — Columbia University, New York, New York 10027, United States

Juan B. Rodriguez III – Columbia University, New York, New York 10027, United States

Gadiel Saper — Columbia University, New York, New York 10027, United States

Complete contact information is available at: https://pubs.acs.org/10.1021/acs.langmuir.0c01002

# **Author Contributions**

N.M.B.K. and H.H. conceived and designed the experiments. N.M.B.K. and J.R. performed the measurements and the data analysis. G.S. performed the IRM experiments. J.R. did the statistical analyses. N.M.B.K. and H.H. wrote the paper. All authors have given approval to the final version of the manuscript.

#### **Notes**

The authors declare no competing financial interest.

# ACKNOWLEDGMENTS

Financial support under NSF grant ENG 1662329 is gratefully acknowledged. This work was performed, in part, at the Center for Integrated Nanotechnologies, an Office of Science User Facility operated for the U.S. Department of Energy (DOE) Office of Science by Los Alamos National Laboratory (contract DE-AC52-06NA25396) and Sandia National Laboratories (contract DE-AC04-94AL85000).

#### REFERENCES

- (1) Hess, H.; Vogel, V. Molecular shuttles based on motor proteins: Active transport in synthetic environments. *Rev. Mol. Biotechnol.* **2001**, 82 (1), 67–85.
- (2) van den Heuvel, M. G. L.; Dekker, C. Motor proteins at work for nanotechnology. *Science* **2007**, 317 (5836), 333–336.
- (3) Wang, J. Can Man-Made Nanomachines Compete with Nature Biomotors? ACS Nano 2009, 3 (1), 4–9.
- (4) Brunner, C.; Wahnes, C.; Vogel, V. Cargo pick-up from engineered loading stations by kinesin driven molecular shuttles. *Lab Chip* **2007**, *7* (10), 1263–1271.
- (5) Schmidt, C.; Vogel, V. Molecular shuttles powered by motor proteins: loading and unloading stations for nanocargo integrated into one device. *Lab Chip* **2010**, *10* (17), 2195–2198.

- (6) Fischer, T.; Agarwal, A.; Hess, H. A smart dust biosensor powered by kinesin motors. *Nat. Nanotechnol.* **2009**, *4*, 162–166.
- (7) Sumino, Y.; Nagai, K. H.; Shitaka, Y.; Tanaka, D.; Yoshikawa, K.; Chate, H.; Oiwa, K. Large-scale vortex lattice emerging from collectively moving microtubules. *Nature* **2012**, *483* (7390), 448–452.
- (8) Nicolau, D. V.; Lard, M.; Korten, T.; van Delft, F. C. M. J. M.; Persson, M.; Bengtsson, E.; Mansson, A.; Diez, S.; Linke, H.; Nicolau, D. V. Parallel computation with molecular-motor-propelled agents in nanofabricated networks. *Proc. Natl. Acad. Sci. U. S. A.* **2016**, *113* (10), 2591–2596.
- (9) Gibbons, F.; Chauwin, J. F.; Desposito, M.; Jose, J. V. A dynamical model of kinesin-microtubule motility assays. *Biophys. J.* **2001**, *80* (6), 2515–26.
- (10) Hess, H.; Matzke, C. M.; Doot, R. K.; Clemmens, J.; Bachand, G. D.; Bunker, B. C.; Vogel, V. Molecular Shuttles Operating Undercover: A New Photolithographic Approach for the Fabrication of Structured Surfaces Supporting Directed Motility. *Nano Lett.* **2003**, 3 (12), 1651–1655.
- (11) Klumpp, S.; Lipowsky, R. Cooperative cargo transport by several molecular motors. *Proc. Natl. Acad. Sci. U. S. A.* **2005**, *102* (48), 17284–9.
- (12) Hancock, W. O.; Howard, J. Processivity of the motor protein kinesin requires two heads. *J. Cell Biol.* **1998**, *140* (6), 1395–1405.
- (13) Fisher, M. E.; Kolomeisky, A. B. Simple mechanochemistry describes the dynamics of kinesin molecules. *Proc. Natl. Acad. Sci. U. S. A.* **2001**, 98 (14), 7748–53.
- (14) Thorn, K. S.; Ubersax, J. A.; Vale, R. D. Engineering the processive run length of the kinesin motor. *J. Cell Biol.* **2000**, *151* (5), 1093–100.
- (15) Clemmens, J.; Hess, H.; Howard, J.; Vogel, V. Analysis of Microtubule Guidance in Open Microfabricated Channels Coated with the Motor Protein Kinesin. *Langmuir* **2003**, *19* (5), 1738–1744.
- (16) Ndlec, F. J.; Surrey, T.; Maggs, A. C.; Leibler, S. Self-organization of microtubules and motors. *Nature* **1997**, 389 (6648), 305–308.
- (17) Palacci, H.; Idan, O.; Armstrong, M. J.; Agarwal, A.; Nitta, T.; Hess, H. Velocity Fluctuations in Kinesin-1 Gliding Motility Assays Originate in Motor Attachment Geometry Variations. *Langmuir* **2016**, 32 (31), 7943–7950.
- (18) Vale, R. D.; Malik, F.; Brown, D. Directional instability of microtubule transport in the presence of kinesin and dynein, two opposite polarity motor proteins. *J. Cell Biol.* **1992**, *119* (6), 1589–1596.
- (19) Howard, J.; Hudspeth, A. J.; Vale, R. D. Movement of microtubules by single kinesin molecules. *Nature* **1989**, 342, 154–158
- (20) Coy, D. L.; Hancock, W. O.; Wagenbach, M.; Howard, J. Kinesin's tail domain is an inhibitory regulator of the motor domain [see comments]. *Nat. Cell Biol.* **1999**, *1* (5), 288–92.
- (21) Dumont, E. L. P.; Do, C.; Hess, H. Molecular wear of microtubules propelled by surface-adhered kinesins. *Nat. Nanotechnol.* **2015**, *10* (2), 166–169.
- (22) Agarwal, A.; Luria, E.; Deng, X.; Lahann, J.; Hess, H. Landing rate measurements of residual fibrinogen adsorption to highly non-fouling surfaces. *Cell. Mol. Bioeng.* **2012**, *5* (3), 320–326.
- (23) Kerssemakers, J.; Ionov, L.; Queitsch, U.; Luna, S.; Hess, H.; Diez, S. 3D Nanometer Tracking of Motile Microtubules on Reflective Surfaces. *Small* **2009**, *5* (15), 1732–1737.
- (24) Boal, A. K.; Bachand, G. D.; Rivera, S. B.; Bunker, B. C. Interactions between cargo-carrying biomolecular shuttles. *Nanotechnology* **2006**, *17* (2), 349–354.
- (25) Saper, G.; Hess, H. Kinesin-propelled label-free microtubules imaged with interference reflection microscopy submitted for publication, 2020.
- (26) Kerssemakers, J.; Howard, J.; Hess, H.; Diez, S. The distance that kinesin holds its cargo from the microtubule surface measured by fluorescence-interference-contrast microscopy. *Proc. Natl. Acad. Sci. U. S. A.* **2006**, *103* (43), 15812–15817.

- (27) Narayan, V.; Ramaswamy, S.; Menon, N. Long-Lived Giant Number Fluctuations in a Swarming Granular Nematic. *Science* **2007**, *317* (5834), 105–108.
- (28) Mahamdeh, M.; Simmert, S.; Luchniak, A.; Schaffer, E.; Howard, J. Label-free high-speed wide-field imaging of single microtubules using interference reflection microscopy. *J. Microsc.* **2018**, 272 (1), 60–66.
- (29) Van Selst, M.; Jolicoeur, P. A Solution to the Effect of Sample Size on Outlier Elimination. Q. J. Exp. Psych. Section A 1994, 47 (3), 631–650.
- (30) Vigers, G. P. A.; Coue, M.; McIntosh, J. R. Fluorescent Microtubules Break Up Under Illumination. *J. Cell Biol.* **1988**, *107*, 1011–1024
- (31) Brunner, C.; Hess, H.; Ernst, K.-H.; Vogel, V. Lifetime of biomolecules in hybrid nanodevices. *Nanotechnology* **2004**, *15* (10), S540–S548.
- (32) Mahamdeh, M.; Simmert, S.; Luchniak, A.; Schaeffer, E.; Howard, J. Label-free high-speed wide-field imaging of single microtubules using interference reflection microscopy. *J. Microsc.* **2018**, 272 (1), 60–66.
- (33) Mahamdeh, M.; Howard, J. Implementation of interference reflection microscopy for label-free, high-speed imaging of microtubules. *J. Visualized Exp.* **2019**, *150*, e59520.
- (34) Nitta, T.; Hess, H. Dispersion in Active Transport by Kinesin-Powered Molecular Shuttles. *Nano Lett.* **2005**, *5* (7), 1337–1342.
- (35) VanDelinder, V.; Imam, Z. I.; Bachand, G. Kinesin motor density and dynamics in gliding microtubule motility. *Sci. Rep.* **2019**, 9 (1), 1–9.
- (36) Korten, T.; Chaudhuri, S.; Tavkin, E.; Braun, M.; Diez, S. Kinesin-1 Expressed in Insect Cells Improves Microtubule in Vitro Gliding Performance, Long-Term Stability and Guiding Efficiency in Nanostructures. *IEEE T Nanobiosci* **2016**, *15* (1), 62–69.
- (37) Gosselin, P.; Mohrbach, H.; Kulić, I. M.; Ziebert, F. On complex, curved trajectories in microtubule gliding. *Phys. D* **2016**, 318–319, 105–111.
- (38) Nitta, T.; Tanahashi, A.; Hirano, M.; Hess, H. Simulating molecular shuttle movements: Towards computer-aided design of nanoscale transport systems. *Lab Chip* **2006**, *6* (7), 881–885.
- (39) Roos, W.; Ulmer, J.; Grater, S.; Surrey, T.; Spatz, J. P. Microtubule Gliding and Cross-Linked Microtubule Networks on Micropillar Interfaces. *Nano Lett.* **2005**, *5* (12), 2630–2634.
- (40) Kaneko, T.; Furuta, K. y.; Oiwa, K.; Shintaku, H.; Kotera, H.; Yokokawa, R. Different motilities of microtubules driven by kinesin-1 and kinesin-14 motors patterned on nanopillars. *Science Advances* **2020**, *6* (4), eaax7413.
- (41) Verma, V.; Hancock, W. O.; Catchmark, J. M. Nanoscale patterning of kinesin motor proteins and its role in guiding microtubule motility. *Biomed. Microdevices* **2009**, *11* (2), 313–322.
- (42) Gittes, F.; Mickey, B.; Nettleton, J.; Howard, J. Flexural rigidity of microtubules and actin filaments measured from thermal fluctuations in shape. *J. Cell Biol.* **1993**, *120* (4), 923–934.
- (43) Amos, L. A.; Cross, R. A. Structure and dynamics of molecular motors. *Curr. Opin. Struct. Biol.* 1997, 7 (2), 239–246.
- (44) Katira, P.; Hess, H. Two-Stage Capture Employing Active Transport Enables Sensitive and Fast Biosensors. *Nano Lett.* **2010**, *10* (2), 567–572.
- (45) Nitta, T.; Hess, H. Effect of Path Persistence Length of Molecular Shuttles on Two-stage Analyte Capture in Biosensors. *Cell. Mol. Bioeng.* **2013**, *6* (1), 109–115.
- (46) Campbell, J.; Paul, D.; Kurabayashi, K.; Meyhofer, E. A Kinesin Driven Enzyme Linked Immunosorbant Assay (ELISA) for Ultra Low Protein Detection Applications. *Biophys. J.* **2014**, *106* (2), *622a*–*622a*.
- (47) Kumar, S.; Milani, G.; Takatsuki, H.; Lana, T.; Persson, M.; Frasson, C.; te Kronnie, G.; Månsson, A. Sensing protein antigen and microvesicle analytes using high-capacity biopolymer nano-carriers. *Analyst* **2016**, *141* (3), 836–846.
- (48) Inoue, D.; Mahmot, B.; Kabir, A. M. R.; Farhana, T. I.; Tokuraku, K.; Sada, K.; Konagaya, A.; Kakugo, A. Depletion force

- induced collective motion of microtubules driven by kinesin. *Nanoscale* **2015**, 7 (43), 18054–18061.
- (49) Farhadi, L.; Fermino Do Rosario, C.; Debold, E. P.; Baskaran, A.; Ross, J. L. Active Self-Organization of Actin-Microtubule Composite Self-Propelled Rods. *Front. Phys.* **2018**, *6*, No. 75.
- (50) Agarwal, A.; Luria, E.; Deng, X. P.; Lahann, J.; Hess, H. Landing Rate Measurements to Detect Fibrinogen Adsorption to Non-fouling Surfaces. *Cell. Mol. Bioeng.* **2012**, *5* (3), 320–326.
- (51) Wettermark, G.; Borglund, E.; Brolin, S. E. A regenerating system for studies of phosphoryl transfer from ATP. *Anal. Biochem.* **1968**, 22 (2), 211–218.
- (52) Ruhnow, F.; Zwicker, D.; Diez, S. Tracking single particles and elongated filaments with nanometer precision. *Biophys. J.* **2011**, *100* (11), 2820–2828.